Volume 12
Number 38
14 October 2021
Pages 12503–12852

Chemical Science

rsc.li/chemical-science

ISSN 2041-6539

ROYAL SOCIETY OF CHEMISTRY

EDGE ARTICLE
Shuhei Furukawa *et al.*
Multiscale structural control of linked metal–organic polyhedra gel by aging-induced linkage-reorganization

Chemical Science

ROYAL SOCIETY OF CHEMISTRY

EDGE ARTICLE

View Article Online
View Journal | View Issue

Cite this: *Chem. Sci.*, 2021, **12**, 12556

All publication charges for this article have been paid for by the Royal Society of Chemistry

Multiscale structural control of linked metal–organic polyhedra gel by aging-induced linkage-reorganization†

Zaoming Wang, [ab] Christian Villa Santos,[c] Alexandre Legrand, [a] Frederik Haase,[a] Yosuke Hara, [d] Kazuyoshi Kanamori, [d] Takuma Aoyama,[e] Kenji Urayama, [e] Cara M. Doherty, [f] Glen J. Smales,[g] Brian R. Pauw,[g] Yamil J. Colón [c] and Shuhei Furukawa *[ab]

Assembly of permanently porous metal–organic polyhedra/cages (MOPs) with bifunctional linkers leads to soft supramolecular networks featuring both porosity and processability. However, the amorphous nature of such soft materials complicates their characterization and thus limits rational structural control. Here we demonstrate that aging is an effective strategy to control the hierarchical network of supramolecular gels, which are assembled from organic ligands as linkers and MOPs as junctions. Normally, the initial gel formation by rapid gelation leads to a kinetically trapped structure with low controllability. Through a controlled post-synthetic aging process, we show that it is possible to tune the network of the linked MOP gel over multiple length scales. This process allows control on the molecular-scale rearrangement of interlinking MOPs, mesoscale fusion of colloidal particles and macroscale densification of the whole colloidal network. In this work we elucidate the relationships between the gel properties, such as porosity and rheology, and their hierarchical structures, which suggest that porosity measurement of the dried gels can be used as a powerful tool to characterize the microscale structural transition of their corresponding gels. This aging strategy can be applied in other supramolecular polymer systems particularly containing kinetically controlled structures and shows an opportunity to engineer the structure and the permanent porosity of amorphous materials for further applications.

Received 27th May 2021
Accepted 20th August 2021

DOI: 10.1039/d1sc02883a

rsc.li/chemical-science

Introduction

Nanoporous materials assembled from metal ions and organic ligands have found a wide range of applications in separation, adsorption, catalysis and gas storage.[1–4] Despite the fact that the majority of such porous metal–organic materials studied to date, also known as metal–organic frameworks (MOFs), have a crystalline state, the limitation in processability has shifted the attention to the fabrication of their amorphous counterparts.[5–8] However, unlike the MOFs that can rely on the periodic linkage of metal ions and ligands to create well-defined micropores, amorphous structures consist of disordered networks with less controlled connectivity, which hampers the design of the pore sizes and shapes especially at the molecular scale.[9–11] To tackle this problem, molecular coordination cages with well-defined internal cavities, such as metal–organic polyhedra/cages (MOPs),[12–14] have been integrated as predesigned porous building blocks into amorphous materials.[15,16] The prerequisite is to introduce connection points (metal ions or functional groups) on the periphery of these cages, allowing their subsequent linkage either by polymers or long alkyl chains.[17–23] The resulting amorphous materials that can be isolated as dried powders,[24] films[25] or wet gels[26] not only retain the rigid cavities of the cages but also possess the mechanical flexibility, processability and functions of the polymers. For example, the introduction of cavity-containing MOPs endows the resulting gels with the ability for selective encapsulation and release of guest molecules.[15] The combination of dynamic coordination bonding of MOPs with the polymer flexibility affords the gel network with photo-switchable topologies and

[a]*Institute for Integrated Cell-Material Science (WPI-iCeMS), Kyoto University, Yoshida, Sakyo-ku, Kyoto 606-8501, Japan. E-mail: shuhei.furukawa@icems.kyoto-u.ac.jp*
[b]*Department of Synthetic Chemistry and Biological Chemistry, Graduate School of Engineering, Kyoto University, Katsura, Nishikyo-ku, Kyoto 615-8510, Japan*
[c]*Department of Chemical and Biomolecular Engineering, University of Notre Dame, Notre Dame, IN 46556, USA*
[d]*Department of Chemistry, Graduate School of Science, Kyoto University, Kitashirakawa, Sakyo-ku, Kyoto 606-8502, Japan*
[e]*Department of Macromolecular Science and Engineering, Kyoto Institute of Technology, Matsugasaki, Sakyo-ku, Kyoto 606-8585, Japan*
[f]*Manufacturing, Commonwealth Scientific and Industrial Research Organisation, Clayton South, Victoria, Australia*
[g]*Bundesanstalt für Materialforschung und -prüfung (BAM), Unter den Eichen 87, 12205 Berlin, Germany*

† Electronic supplementary information (ESI) available. See DOI: 10.1039/d1sc02883a

responsiveness.[27,28] Recently we reported the fabrication of wet gels with hierarchical porous structures by coordinatively linking cuboctahedral MOPs, $[Rh_2(bdc)_2]_{12}$ (**HRhMOP**; bdc = benzene-1,3-dicarboxylate), with bidentate linkers, **bix** (1,4-bis(imidazol-1-ylmethyl)benzene).[29,30] The high structural stability of **HRhMOP** with intact cavity results in processable gels that are able to withstand the harsh desolvation process to form the corresponding aerogels with permanent microporosity. Despite these achievements, it is still challenging to further characterize and control the permanent porosity of these linked MOPs inside the resulting dried gel materials. This is because of the lack of fixed directionality and defined topology within the molecular networks, in which the cages are inhomogeneously distributed and thus their crosslinking is hard to control.[31] Besides the isolated cage cavities, the supramolecular arrangement of cages and the connections between them determine the accessible porosity of the materials. When polymer linkers are used to connect cages, the polymers tend to pack densely to minimize the empty spaces (or voids) in the dried state and inhibit the molecular diffusion throughout the materials.[32] Therefore, the development of methods is required to not only incorporate but also further characterize and engineer the permanent microporosity of the linked MOPs in these amorphous materials.

Efforts to manipulate the porous networks of crystalline MOF materials have been intensively made based on the strategy of post-synthetic modification (PSM).[33,34] Thanks to the reversibility of the coordination bonds that dominate the connectivity of metal ions and organic ligands, even after their formation the porous structures and properties of MOFs can be precisely tailored by functionalizing,[35] swapping,[36] eliminating or newly introducing building blocks.[37] When looking at the metal–organic soft materials, in particular gels, the PSM would give a new opportunity to tune their structures. This is because gels contain solvents therein, which ensure the dynamics of reversible coordination bond formation/dissociation for further PSM. Indeed, gels are often prepared in metastable states, which are trapped at the local energy minima.[38–41] By post-synthetically importing external stimuli (like heat, pH and photo-irradiation), structural transitions can be induced from one trapped state to another metastable state, allowing further structural control.[42–45]

One typical example is the aging treatment of gels.[46] In most cases the gelation process is not performed under thermodynamic control so that the obtained gels inevitably show certain aging behaviours with time-dependent changes in the chemical or physical structure of materials.[47] Despite being mostly recognized as an uncontrollable spontaneous process in polymer materials,[48] aging has been utilized as a tool in the sol–gel chemistry to improve the performance of gels by intentionally intervening the aging process.[49,50] For example, by aging as-synthesized silica gels under controlled temperature, solvent or pH conditions, further chemical reactions involving the remaining unbound oligomers or monomers can be triggered, leading to mesoscale structural rearrangements with increased size of colloidal particles and density of silica gels.[50,51] For the supramolecular gel systems including metal–organic gels, however, the exploration of aging on their structural control is quite rare. Although there are some reports about their gel-to-gel or gel-to-crystal transitions over time,[52,53] most studies only focused on the gel morphology at the mesoscale, where the influence of the structural changes on the macroscale properties like transparency and stiffness are readily apparent.[54] It is still challenging to understand the effect of aging on the relationship between structures and properties at the molecular scale because of the difficulty in characterizing structural transitions of the amorphous materials/gels.

Here we demonstrate that the aging process can effectively control the hierarchical structures of the linked **HRhMOP** gels by inducing gradual structural transitions. By heating the as-synthesized gels in fresh solvent, aging process was performed to induce further crosslinking of MOPs inside the network, leading to a controllable transition of the whole structure over multiple length scales (Fig. 1). This transition is characterized by: (1) molecular-scale rearrangement of the crosslinked MOPs generated more-defined extrinsic microporosity. (2) Further connection of mesoscale colloidal particles resulted in a higher packing density. (3) Macroscale densification of the gel networks led to a shrinkage and increased stiffness. By repeating the aging process, we show that the corresponding gel structures and properties can be tailored. Combined with simulation and sorption measurements, we demonstrate a way to characterize the effect of aging on the molecular-scale network rearrangements and thus the permanent microporosity.

Results and discussion

Preparation of the linked MOP gels and the subsequent aging process

The gels made from **HRhMOP** are attractive targets because the thermal stability of the MOPs allow their internal cavities to be maintained after desolvation process.[30] In contrast to other MOP gels which incorporate polymers as linkers, the use of the short linker **bix** affords a well-defined hierarchical structure over multiple length scales: isolated MOP cages are crosslinked by **bix** at the molecular scale, leading to the formation of mesoscale colloidal particles (around 25 nm), followed by their further fusion and percolation to give a colloidal gel network (Fig. 1).[30,52] The resulting linked MOP network consists of multiscale porosities as molecular MOP cavities, mesoscale external pores between linked MOPs inside the colloids and macropores of the colloidal network. Such hierarchical structure affords optimal molecular diffusion throughout the material to demonstrate permanent porosity for gas sorption.

The gel samples were synthesized through previously reported coordinative solubilizer method.[30] Through reversibly attaching a coordinatively monodentate ligand, **diz** (1-dodecyl-1*H*-imidazole), to the exohedral Rh sites of **HRhMOP**, solubility of the resulting $\mathbf{HRhMOP(diz)_{12}}$ in DMF was greatly increased. Then these monodentate **diz** were replaced with nominally bidentate linker **bix** in DMF through ligand–exchange reaction, forming the so-called kinetically trapped molecules as $\mathbf{HRhMOP(bix)_{10}(diz)_2}$ with **bix** coordinating in a monodentate

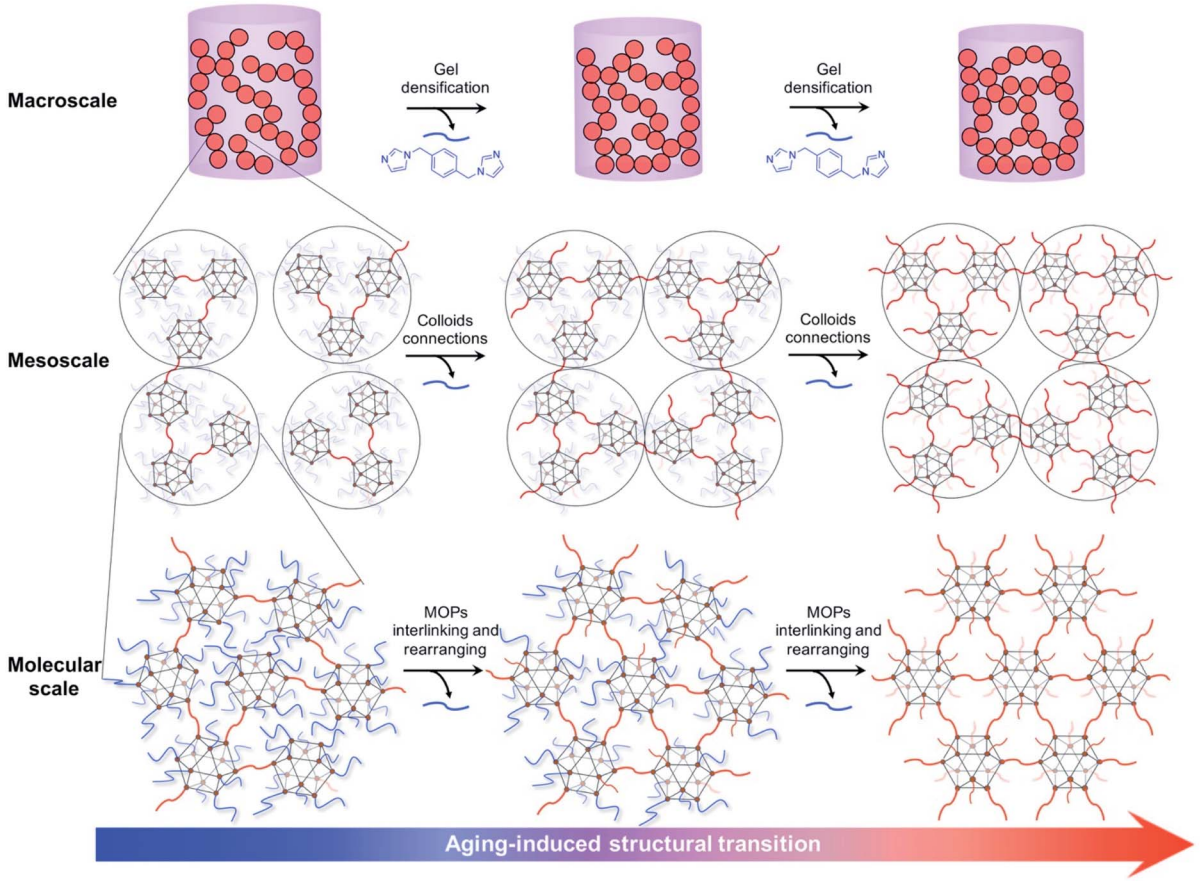

Fig. 1 Schematic illustration of influence of aging on the hierarchical structure of linked MOP gel at multiple length scales. The **bix** molecules which coordinate in a monodentate fashion are drawn in blue, while the **bix** linkers that crosslink MOPs to form network are drawn in red. The **diz** molecules are not plotted here for simplification. During repeating aging process, excessive amount of imidazole ligands (**bix** and **diz**) dissociated from the MOP surfaces into the solvent, leading to the generation of exposed Rh sites which were subsequently linked with remaining **bix** from neighboring MOPs. This further crosslinking of MOPs induced the structural transition of gel networks over multiple length scales, including the molecular-scale rearrangement of interlinking MOPs, mesoscale fusion of colloidal particles and macroscale densification of the whole colloidal network as illustrated here.

fashion (Fig. S2 and S3†). Heating the solution of the kinetically trapped molecules at 80 °C drove the assembly of MOPs into porous gels by the dissociation of excessive imidazole ligands and the subsequent crosslinking of MOPs with remaining **bix**.[55] In a typical reaction here, 1.4 mM kinetically trapped molecules were used to lead to the formation of gels within a few minutes (Fig. S4†). To characterize the materials, the corresponding aerogel was prepared by solvent exchange from DMF to acetone, followed by supercritical CO_2 drying. Based on the ^{1}H NMR analysis of the digested aerogel, the composition of as-synthesized gel was estimated to be **HRhMOP(bix)$_{9.4}$(diz)$_{1.1}$** (Fig. S5†). Assuming that all 12 exohedral Rh sites of MOPs in the gel network were coordinated by the imidazole ligands (**bix** or **diz**), the network branch functionality of the gel, f, which is the average number of exohedral Rh sites per MOP used as bridges to crosslink with neighbouring MOPs,[16] is calculated to be as low as 3.0 (Table 1, see details of calculation in ESI†). This low f value indicates that a large amount of monodentate **bix** and a small amount of **diz** remained in the whole network. It is thus hypothesized that the crosslinking reaction of MOPs was trapped at the initial stage.

For a typical aging cycle, fresh solvent (DMF) was added to the gels, followed by heating at 80 °C for 8 h. By cycling this aging process, gels with different aging degrees were obtained and referred henceforth as **Gel-*n*** (n indicates the number of aging cycles). These gels were then dried by supercritical CO_2 to obtain their corresponding aerogels (named as **Aerogel-*n***). The

Table 1 Composition and the corresponding branch functionality, f, of gels after treatment of different aging cycles

Sample	Composition	f
Gel-0	HRhMOP(bix)$_{9.4}$(diz)$_{1.1}$	3.0
Gel-1	HRhMOP(bix)$_{8.8}$(diz)$_{1.0}$	4.4
Gel-2	HRhMOP(bix)$_{8.6}$(diz)$_{0.9}$	5.0
Gel-3	HRhMOP(bix)$_{8.3}$(diz)$_{0.8}$	5.8
Gel-4	HRhMOP(bix)$_{8.1}$(diz)$_{0.7}$	6.4
Gel-5	HRhMOP(bix)$_{8.0}$(diz)$_{0.7}$	6.6

effect of the aging process on the composition of each aged sample was determined by the ^{1}H NMR experiments of the digested aerogels (Fig. S5†). From the results of ^{1}H NMR it is apparent that during each aging cycle, the number of imidazole ligands (**bix** and **diz**) per MOP inside the gel network is reduced (Table 1). The continuous removal or dissociation of these ligands from MOP exposed free Rh sites which could be subsequently linked by remaining **bix** from neighbouring MOPs for further crosslinking. Assuming that all exohedral Rh sites of MOPs were coordinated by the ligands, the value of f was calculated to present a significant increase from 3.0 for **Gel-0** to 6.6 for **Gel-5** (Table 1). In addition, the continuous removal of **bix** during repeated aging cycles was also confirmed by infrared spectroscopy (IR) (Fig. S6†); the related ratio of the characteristic peaks for **bix** and **HRhMOP** displayed the similar trend as observed from ^{1}H NMR. To demonstrate the reproducibility of the aging process, different batches of gel samples were synthesized and the ^{1}H NMR analysis was performed to estimate the composition along with aging cycles. The average composition of each **Gel-*n*** was summarized in Table S1,† which showed the same composition and the f evolution during aging as discussed above. In the next sections, the influences of the change of f on the gel structures and properties over multiple length scales are discussed in detail.

Structural transition of the linked MOP gels at macro- and mesoscale

Visual inspection of the gel after aging treatment revealed a shrinkage with the height of as-synthesized gel decreasing from 1.2 cm for **Gel-0** to 1.0 cm for **Gel-2** after two aging cycles (Fig. 2a). Further aging processes showed only negligible change in size with the height of **Gel-5** to be 1.0 cm (Fig. S7†). Scanning electron microscopy (SEM) reveals that in the colloidal network of **Aerogel-2** the colloidal particles were more densely packed than those in the **Aerogel-0** network (Fig. 2b and c). Consistent with the shrinkage behavior, aerogels treated with increased numbers of aging cycles presented similar colloidal packing density to **Aerogel-2** (Fig. S8 and S9†). This result indicated that the gel shrinkage or densification after aging was attributed to the increasing connection between colloidal nanoparticles, which could be triggered through the further crosslinking of MOPs by **bix** at their interface. To confirm the hypothesis, rheology measurements in a compression mode were performed by considering that the mechanical property of the gels is dominated by the fusion or interaction of colloidal particles.[56–58] As shown in Fig. 3a and S10,† the gel samples were observed to show an increased mechanical stiffness upon aging especially at the first two aging cycles; **Gel-2** has a higher storage Young's modulus E' (~3.3 kPa) than the as-synthesized **Gel-0** (~1.9 kPa). However, this increase seems to saturate when continuing the aging process above 2 cycles (E' = ~3.4 kPa for **Gel-5**), which in accordance with above results confirms the close relationship between colloidal connection and the resulting gel stiffness.

The major change in gel size and stiffness was only observed at the first two aging cycles, despite the continuous increase of f for gels with higher aging degrees (Fig. 3a). Considering the hierarchical structures of the gels, aging should induce crosslinking of MOPs not only at the interface of colloidal particles but also within them. The MOP crosslinking at the colloidal interfaces resulted in the mesoscale connection of colloidal particles, giving a macroscopic denser gel structure with higher stiffness. However, this relinkage is restricted by the flexibility of the whole gel network. With the increase of f, the gel became denser and the colloidal particles in the network were fixed with each other through increasing connections, restricting their further packings. In contrast, the MOP crosslinking inside the colloidal particles could continuously occur without having a major impact on their flexibility. Instead of changing the gel properties at the meso- and macroscale, the rearrangement of interlinked MOPs inside each colloid would rather exert the influences at the molecular scale, the studies of which are discussed in the following sections.

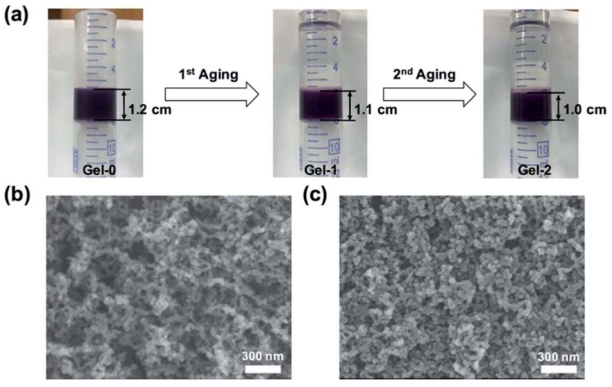

Fig. 2 (a) Pictures of the gel shrinkage during first two aging cycles. SEM images of (b) Aerogel-0 and (c) Aerogel-2.

Structural rearrangement of the linked MOP network at the molecular scale

To further understand the molecular-scale structural rearrangement during the aging process, small-/wide-angle X-ray scattering (SAXS/WAXS) of all aerogels was performed as shown in Fig. 3b (see Fig. S11a† with all data on an absolute intensity scale). Fitting of the SAXS data by power-law approximation was applied to obtain information on the fractal structures of the linked MOP gels (Fig. S12 and S13†).[59] Especially, the approximation of the low-q data (0.012–0.1 nm^{-1}) reveals a mass fractal dimension (the negative slope) between 1.45–1.85 for all aerogel samples (Table S2†), implying that the gelation of MOPs follows the diffusion-limited cluster aggregation (DLCA).[60] In the high-q region (0.2–2 nm^{-1}), a noticeable change of the slope was observed from the neat **HRhMOP** ($q^{-3.2}$) to the aerogel samples ($q^{-3.78}$ for **Aerogel-0**), indicating a smoother surface of MOP-linked particles than the physical MOP aggregates.[61] After aging, a slight increase of slope was observed from −3.78 for **Aerogel-0** to −3.83 for **Aerogel-5**, which suggests a further decreased surface roughness of the colloidal particles (Table S2†). This change in roughness was attributed to the

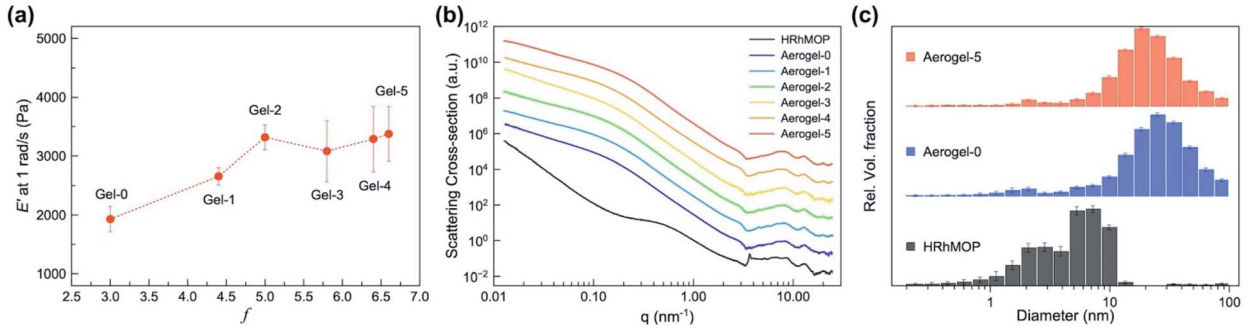

Fig. 3 (a) Evolution of storage Young's modulus (E' at 1 rad s^{-1}) of **Gel-*n*** as a function of f during repeated aging process. (b) SXAX/WAXS curves of **HRhMOP** and **Aerogel-*n*** (the data was stacked for clarity, all data on an absolute intensity scale can be found in ESI†). (c) Form-free size distributions of **HRhMOP**, **Aerogel-0** and **Aerogel-5** extracted from SAXS fits from Monte Carlo method.

increasing branch functionality by aging process, together with the above results confirming the structural transition of the gel systems.

Besides the power-law approximation, the analysis of the SAXS data by Monte Carlo methods (McSAS) allows for the extraction of form-free size distribution,[62] revealing information of the gel structures at different scales (Fig. S14 and S15†). For **Aerogel-*n*** samples, two populations were observed in the corresponding size distribution histograms (Fig. 3c and S16,† the data summarized in Table S2†): (1) the small population has a volume-weighted mean diameter of ~1.7 nm, in accordance with the size of the neat **HRhMOP** with a mean diameter at 1.9 nm. (2) The larger population, on the other hand, has a mean diameter above 23 nm, which well matches the dimensions of the colloidal particles observed from the SEM images of the gel network (Fig. S8 and S9†). After aging, the average diameter of the colloidal particles was reduced from 28.4 nm for **Aerogel-0** to 23.6 nm for **Aerogel-5**, implying a densification of these particles (Table S2†). Similar to the shrinkage of the gel networks that was attributed to the aging-induced connection of MOPs at the colloidal surfaces, the size reduction in each colloid was explained by the further crosslinking of MOPs inside the colloidal particles (Fig. 1 and S22†). Note that MOP crosslinking might not be the only reason for the colloidal densification. Due to the removal of imidazole ligands (**bix** and **diz**), the particles are supposed to possess more free volume, which might be lost during the drying process and result in the reduction in the final particle size. To further confirm the MOPs crosslinking or rearrangement inside the colloidal particles, porosity of the aged gel networks was studied.

Enhancement of microporosity in the amorphous network of the linked MOP gels by aging

The rearrangement of the linked MOP structure insides the colloids are expected to influence the microporosity of the gels, which was studied by performing N_2 sorption of three dried aerogel samples, **Aerogel-0**, **Aerogel-2** and **Aerogel-5** at 77 K (Fig. 4a). Compared to the neat **HRhMOP**, all aerogel samples show much higher N_2 capacity especially in the high-pressure region, arising from the macropores and mesopores of the gel network: **HRhMOP** adsorbs 94 moles of N_2 per mole of MOP while **Aerogel-0** adsorbs 427 moles of N_2 per mole of MOP at P/P_0 ~1.

By repeating the aging cycles, a continuous increase in the Brunauer–Emmett–Teller (BET) surface area was observed from 565 $m^2\ g^{-1}$ (**Aerogel-0**) to 758 $m^2\ g^{-1}$ (**Aerogel-5**), corresponding to the removal of monodentate ligands that occupied the voids between MOPs (Table S3†). In contrast, the total pore volume of the aerogels exhibited a different trend during aging treatment. Compared to **Aerogel-0** with a total pore volume of 1.66 $cm^3\ g^{-1}$, **Aerogel-2** showed a smaller pore volume of 1.42 $cm^3\ g^{-1}$, consistent with the gel shrinkage/densification during the first two aging cycles. Further aging process resulted in an increased volume to 1.77 $cm^3\ g^{-1}$ for **Aerogel-5**, which is attributed to the removal of monodentate ligands and to the rearrangement of linked MOP cages inside each colloidal particle. These results show that the aging process plays an important role in tuning the porosity of the linked MOP system post-synthetically.

Unlike flexible polymers that normally pack densely to block the intrinsic porosity of MOPs,[25] the crosslinking of MOPs with the shorter linker, **bix**, creates the external pores between MOPs, through which the connection of MOP cavities and thus access to their internal cavities is guaranteed by the molecular diffusion (Fig. 1 and S22†). This feature not only affords the permanent porosity, but also offers the possibility to control the microporosity of the gel network by rearranging interlinking MOPs. At 77 K, both **HRhMOP** and **Aerogel-*n*** display a sharp uptake of N_2 at low pressure, characteristic of microporous materials (see logarithmic data in Fig. S18†). Pore size distribution (PSD) was calculated by using nonlocal density functional theory (NLDFT), as shown in Fig. 4b. The PSD of **HRhMOP** reveals two micropores with size centered at 0.7 nm and 1.2 nm, which are assigned to the intrinsic MOP cavities and the interstitial space between randomly packed MOPs, respectively (Fig. S20†).[63] In contrast, all **Aerogel-*n*** exhibit a hierarchical porosity of the linked-MOP networks with different pore sizes centered at micro- and mesoporous regions. A micropore is observed with the size centered at *ca.* 0.6 nm, indicating the preservation of MOP cavities in the amorphous network after gelation and aging. Similar pore size at ~0.66 nm

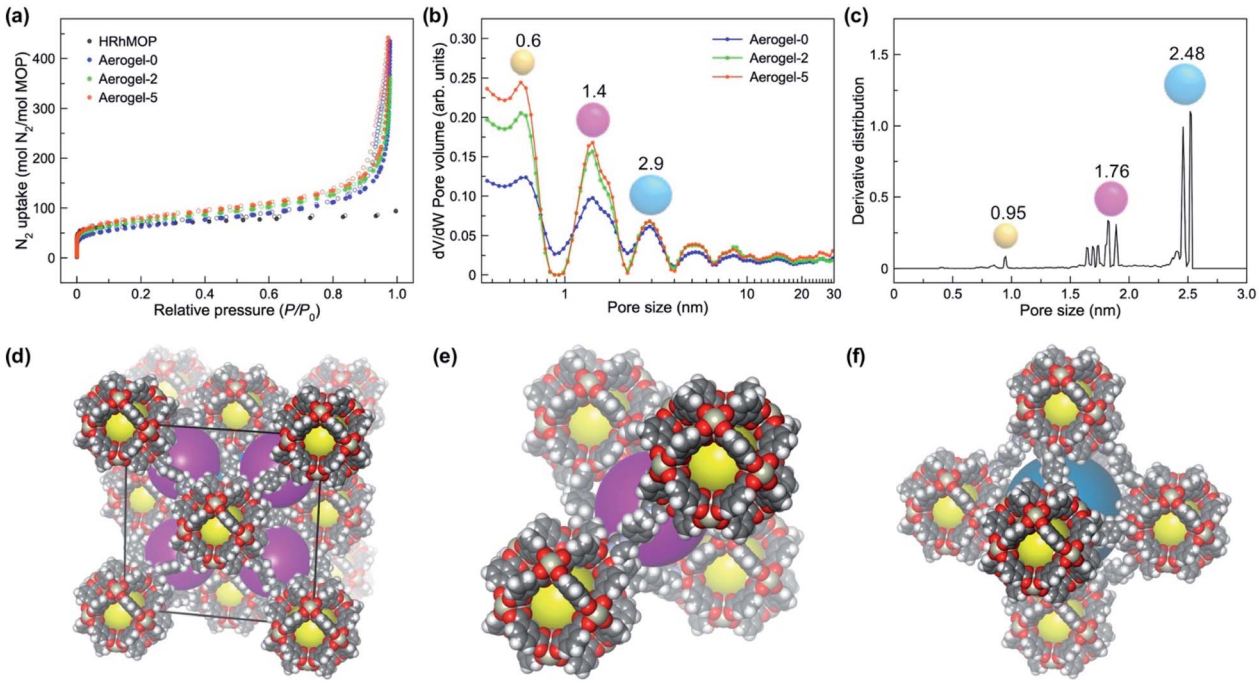

Fig. 4 (a) N_2 adsorption isotherm at 77 K for **Aerogel-0**, **Aerogel-2**, **Aerogel-5** and **HRhMOP** with adsorption plot in filled circles and desorption plot in unfilled circles. (b) The corresponding pore size distribution (PSD) estimated from N_2 isotherm by NLDFT on a slit pore model. (c) Simulated pore size distribution (PSD) of the ideal crystalline network of the linked MOPs with **fcu** topology, named **HRhMOP(bix)$_6$**, in which each **HRhMOP** was linked by 12 **bix**. (d) Simulated crystalline structure of **HRhMOP(bix)$_6$**, which was minimized by geometry optimization using the LAMMPS software. The elements of C, H, O, N, Rh are drawn in sphere of gray, white, red, light blue and tan, respectively. (e and f) Perspective view of the three different pores in the ideal linked MOP networks with $f = 12$ with colors in yellow, pink and blue, respectively.

was also observed in the positron annihilation lifetime spectroscopy (PALS) experiments, confirming the intact nature of MOP inside the gel network (Table S4 and Fig. S21†). In addition, two larger pores emerge in the PSD of all aerogel samples with the diameter of 1.4 and 2.9 nm, which can be assigned to the pores between the interlinked MOPs (Fig. S22b†). After aging, the aerogel samples show a clear increase in the volume of micropores with the size at 0.6 and 1.4 nm, indicating the enhancement of gel microporosity by aging process. Note that similar two pore sizes at ~0.50 nm and ~1.36 nm in **Aerogel-*n*** could also be obtained from the peaks of WAXS curves, in which the bigger pore showed a decrease in size from 1.36 nm for **Aerogel-0** to 1.30 nm for **Aerogel-5** (Fig. S11 and Table S5†), suggesting a more crosslinked MOP networks by **bix** as increasing aging degrees.

To correlate the microporosity of aged aerogels with the rearrangement process of interlinking MOPs, an ideal model of the linked MOP network was computed at an extreme condition of $f = 12$ (Fig. 4d). With all 12 exohedral Rh sites per MOP bonded as coordinative connections with linker **bix**, a crystalline structure with **fcu** topology, named as **HRhMOP(bix)$_6$**, was constructed and its porosity was explored by simulating the corresponding gas adsorption (full details are given in ESI†). **HRhMOP(bix)$_6$** presents a higher gas uptake in the N_2 isotherm than **Aerogel-5**, which can be explained by its much higher ordered microporosity than that of amorphous aerogels (Fig. S24†). The PSD simulation of the ideal **HRhMOP(bix)$_6$** reveals three populations of pores in the similar size range as the aged aerogels (Fig. 4c): the smallest pores around 0.95 nm corresponds to MOP cavities, while the other two populations of pores around 1.76 nm and 2.48 nm corresponds to the truncated tetrahedral and octahedral pores which are interconnected through triangular and square windows of adjacent MOPs, respectively (Fig. 4e and f). This distribution matches well with the PSD obtained experimentally in the aged aerogels, which allows us to propose two reasons to explain the dependency of porosity on aging: (1) the removal of monodentate **bix** or **diz** weakens their blocking effect on MOPs, entailing more MOP cavities accessible towards gas sorption; (2) as higher f is achieved by continuous aging, MOPs inside each colloidal particle are rearranged by relinkage, "transforming" the initially random MOP aggregates into a more porous network (Fig. 1 and S22†). As a result, an enhancement in porosity was observed after aging and the aged samples presented a more distinguishable pore distribution.

Conclusions

In summary, we have demonstrated a strategy to control the structures and properties of the MOP-linked supramolecular gels in multiple length scales. By simply aging the gels, coordination equilibrium is directed into a gel network with higher branch functionality, f, leading to the rearrangement of interlinking MOPs and thus microporosity enhancement at the

molecular scale. Simultaneously, more colloidal particles are connected with each other at the mesoscale due to the interlinking of MOPs at their surfaces, resulting in the formation of a denser gel network with enhanced mechanical properties at the macroscale. Interestingly, this controlled dissociation and relinkage of linkers during aging process shows the possibility for further exchange with new ligands, allowing for additional modification on the gel network, such as the incorporation of functional groups or the creation of a second network by full use of the coordination chemistry. As a powerful post-synthetic strategy, aging process offers a feasible way to tune the structure of the linked MOP systems, allowing us to control both structures and properties of these amorphous porous soft materials for further application.

Data availability

All experimental and simulation data and detailed procedures are available in ESI.†

Author contributions

Z. W. and S. F. conceived and designed the project. Z. W. performed all synthetic experiments. Z. W., A. L. and F. H. performed dynamic light scattering experiments. Z. W., Y. H. and K. K. performed materials' density characterization. Z. W., T. A. and K. U. performed rheology experiments. C. M. D. performed positron annihilation lifetime spectroscopy experiments. G. J. M. and B. R. P performed small-angle X-ray scattering experiments. C. V. S. and Y. J. C. performed computational simulation. Z. W. and S. F. wrote the manuscript. All authors discussed the results and commented on the manuscript.

Conflicts of interest

The authors declare that they have no competing financial interests.

Acknowledgements

Z. W. acknowledges the China Scholarship Council (CSC) for the scholarship support. This study was supported by JSPS KAKENHI Grant Number 20K15366 (Wakate) for A. L. and 19H04575 (Coordination Asymmetry) and 18H01995 (Kiban B) for S. F. C. M. D acknowledges support from the Veski Inspiring Women Fellowship. F. H. is grateful to the Japan Society for the Promotion of Science (JSPS) for the Post-Doctoral Fellowship. The authors thank Dr Eli Sanchez-Gonzalez and Mr Shun Tokuda for helping the schematic illustration and the iCeMS Analysis Center for access to analytical instruments.

Notes and references

1 J. S. Seo, D. Whang, H. Lee, S. I. Jun, J. Oh, Y. J. Jeon and K. Kim, *Nature*, 2000, **404**, 982–986.
2 M. E. Davis, *Nature*, 2002, **417**, 813–821.
3 S. Kitagawa, R. Kitaura and S.-i. Noro, *Angew. Chem., Int. Ed.*, 2004, **43**, 2334–2375.
4 H. Furukawa, K. E. Cordova, M. O'Keeffe and O. M. Yaghi, *Science*, 2013, **341**, 1230444.
5 A. G. Slater and A. I. Cooper, *Science*, 2015, **348**, aaa8075.
6 T. D. Bennett and S. Horike, *Nat. Rev. Mater.*, 2018, **3**, 431–440.
7 N. Hosono and S. Kitagawa, *Acc. Chem. Res.*, 2018, **51**, 2437–2446.
8 J. Hou, A. F. Sapnik and T. D. Bennett, *Chem. Sci.*, 2020, **11**, 310–323.
9 S. Jiang, J. T. Jones, T. Hasell, C. E. Blythe, D. J. Adams, A. Trewin and A. I. Cooper, *Nat. Commun.*, 2011, **2**, 1–7.
10 S. Das, P. Heasman, T. Ben and S. Qiu, *Chem. Rev.*, 2017, **117**, 1515–1563.
11 A. Carné-Sánchez, G. A. Craig, P. Larpent, T. Hirose, M. Higuchi, S. Kitagawa, K. Matsuda, K. Urayama and S. Furukawa, *Nat. Commun.*, 2018, **9**, 1–8.
12 S. J. Dalgarno, N. P. Power and J. L. Atwood, *Coord. Chem. Rev.*, 2008, **252**, 825–841.
13 D. J. Tranchemontagne, Z. Ni, M. O'Keeffe and O. M. Yaghi, *Angew. Chem., Int. Ed.*, 2008, **47**, 5136–5147.
14 A. J. Gosselin, C. A. Rowland and E. D. Bloch, *Chem. Rev.*, 2020, **120**, 8987–9014.
15 J. A. Foster, R. M. Parker, A. M. Belenguer, N. Kishi, S. Sutton, C. Abell and J. R. Nitschke, *J. Am. Chem. Soc.*, 2015, **137**, 9722–9729.
16 A. V. Zhukhovitskiy, M. Zhong, E. G. Keeler, V. K. Michaelis, J. E. Sun, M. J. Hore, D. J. Pochan, R. G. Griffin, A. P. Willard and J. A. Johnson, *Nat. Chem.*, 2016, **8**, 33.
17 X. Yan, T. R. Cook, J. B. Pollock, P. Wei, Y. Zhang, Y. Yu, F. Huang and P. J. Stang, *J. Am. Chem. Soc.*, 2014, **136**, 4460–4463.
18 K. Kawamoto, S. C. Grindy, J. Liu, N. Holten-Andersen and J. A. Johnson, *ACS Macro Lett.*, 2015, **4**, 458–461.
19 D. Nam, J. Huh, J. Lee, J. H. Kwak, H. Y. Jeong, K. Choi and W. Choe, *Chem. Sci.*, 2017, **8**, 7765–7771.
20 J. Uchida, M. Yoshio, S. Sato, H. Yokoyama, M. Fujita and T. Kato, *Angew. Chem., Int. Ed.*, 2017, **56**, 14085–14089.
21 J. Liu, W. Duan, J. Song, X. Guo, Z. Wang, X. Shi, J. Liang, J. Wang, P. Cheng, Y. Chen, M. J. Zaworotko and Z. Zhang, *J. Am. Chem. Soc.*, 2019, **141**, 12064–12070.
22 M. A. Andrés, A. Carné-Sánchez, J. Sánchez-Laínez, O. Roubeau, J. Coronas, D. Maspoch and I. Gascón, *Chem.–Eur. J.*, 2020, **26**, 143–147.
23 R.-J. Li, C. Pezzato, C. Berton and K. Severin, *Chem. Sci.*, 2021, **12**, 4981–4984.
24 G. Lal, M. Derakhshandeh, F. Akhtar, D. M. Spasyuk, J.-B. Lin, M. Trifkovic and G. K. H. Shimizu, *J. Am. Chem. Soc.*, 2019, **141**, 1045–1053.
25 T.-H. Chen, L. Wang, J. V. Trueblood, V. H. Grassian and S. M. Cohen, *J. Am. Chem. Soc.*, 2016, **138**, 9646–9654.
26 L. Shao, B. Hua, X. Hu, D. Stalla, S. P. Kelley and J. L. Atwood, *J. Am. Chem. Soc.*, 2020, **142**, 7270–7275.
27 Y. Gu, E. A. Alt, H. Wang, X. Li, A. P. Willard and J. A. Johnson, *Nature*, 2018, **560**, 65–69.

28 N. J. Oldenhuis, K. P. Qin, S. Wang, H.-Z. Ye, E. A. Alt, A. P. Willard, T. Van Voorhis, S. L. Craig and J. A. Johnson, *Angew. Chem., Int. Ed.*, 2020, **59**, 2784–2792.
29 S. Furukawa, N. Horike, M. Kondo, Y. Hijikata, A. Carné-Sánchez, P. Larpent, N. Louvain, S. Diring, H. Sato and R. Matsuda, *Inorg. Chem.*, 2016, **55**, 10843–10846.
30 A. Carné-Sánchez, G. A. Craig, P. Larpent, V. Guillerm, K. Urayama, D. Maspoch and S. Furukawa, *Angew. Chem., Int. Ed.*, 2019, **131**, 6413–6416.
31 P. Jeyakkumar, Y. Liang, M. Guo, S. Lu, D. Xu, X. Li, B. Guo, G. He, D. Chu and M. Zhang, *Angew. Chem., Int. Ed.*, 2020, **59**, 15199–15203.
32 N. B. McKeown and P. M. Budd, *Macromolecules*, 2010, **43**, 5163–5176.
33 Z. Yin, S. Wan, J. Yang, M. Kurmoo and M.-H. Zeng, *Coord. Chem. Rev.*, 2019, **378**, 500–512.
34 M. Kalaj and S. M. Cohen, *ACS Cent. Sci.*, 2020, **6**, 1046–1057.
35 Z. Wang and S. M. Cohen, *J. Am. Chem. Soc.*, 2007, **129**, 12368–12369.
36 B. J. Burnett, P. M. Barron, C. Hu and W. Choe, *J. Am. Chem. Soc.*, 2011, **133**, 9984–9987.
37 B. Tu, Q. Pang, D. Wu, Y. Song, L. Weng and Q. Li, *J. Am. Chem. Soc.*, 2014, **136**, 14465–14471.
38 J. Boekhoven, J. M. Poolman, C. Maity, F. Li, L. van der Mee, C. B. Minkenberg, E. Mendes, J. H. van Esch and R. Eelkema, *Nat. Chem.*, 2013, **5**, 433–437.
39 E. Mattia and S. Otto, *Nat. Nanotechnol.*, 2015, **10**, 111–119.
40 D. B. Amabilino, D. K. Smith and J. W. Steed, *Chem. Soc. Rev.*, 2017, **46**, 2404–2420.
41 T. Fukui, S. Kawai, S. Fujinuma, Y. Matsushita, T. Yasuda, T. Sakurai, S. Seki, M. Takeuchi and K. Sugiyasu, *Nat. Chem.*, 2017, **9**, 493–499.
42 S. Yagai, M. Yamauchi, A. Kobayashi, T. Karatsu, A. Kitamura, T. Ohba and Y. Kikkawa, *J. Am. Chem. Soc.*, 2012, **134**, 18205–18208.
43 A. Lavrenova, D. W. R. Balkenende, Y. Sagara, S. Schrettl, Y. C. Simon and C. Weder, *J. Am. Chem. Soc.*, 2017, **139**, 4302–4305.
44 B. Adhikari, K. Aratsu, J. Davis and S. Yagai, *Angew. Chem., Int. Ed.*, 2019, **58**, 3764–3768.
45 M. Wehner and F. Würthner, *Nat. Rev. Chem.*, 2020, **4**, 38–53.
46 J. V. Alemán, A. V. Chadwick, J. He, M. Hess, K. Horie, R. G. Jones, P. Kratochvíl, I. Meisel, I. Mita, G. Moad, S. Penczek and R. F. T. Stepto, *Pure Appl. Chem.*, 2007, **79**, 1801–1829.
47 E. R. Draper, T. O. McDonald and D. J. Adams, *Chem. Commun.*, 2015, **51**, 6595–6597.
48 L. C. E. Struik, *Physical Aging in Amorphous Polymers and Other Materials*, Elsevier Scientific Publication Co., Amsterdam, 1978.
49 A. M. Fuentes-Caparrós, F. de Paula Gómez-Franco, B. Dietrich, C. Wilson, C. Brasnett, A. Seddon and D. J. Adams, *Nanoscale*, 2019, **11**, 3275–3280.
50 M. A. Aegerter, N. Leventis and M. M. Koebel, *Aerogels Handbook*, Springer, New York, 2011.
51 D. Levy and M. Zayat, *The Sol–Gel Handbook, 3 Volume Set: Synthesis, Characterization, and Applications*, Wiley, 2015.
52 Y. Wang, R. M. de Kruijff, M. Lovrak, X. Guo, R. Eelkema and J. H. van Esch, *Angew. Chem., Int. Ed.*, 2019, **58**, 3800–3803.
53 T. Guterman, M. Levin, S. Kolusheva, D. Levy, N. Noor, Y. Roichman and E. Gazit, *Angew. Chem., Int. Ed.*, 2019, **58**, 15869–15875.
54 S. Panja and D. J. Adams, *Chem. Soc. Rev.*, 2021, **50**, 5165–5200.
55 A. Legrand, G. A. Craig, M. Bonneau, S. Minami, K. Urayama and S. Furukawa, *Chem. Sci.*, 2019, **10**, 10833–10842.
56 P. J. Lu, E. Zaccarelli, F. Ciulla, A. B. Schofield, F. Sciortino and D. A. Weitz, *Nature*, 2008, **453**, 499–503.
57 L. C. Hsiao, R. S. Newman, S. C. Glotzer and M. J. Solomon, *Proc. Natl. Acad. Sci. U. S. A.*, 2012, **109**, 16029.
58 J. D. Park and K. H. Ahn, *Soft Matter*, 2013, **9**, 11650–11662.
59 E. G. R. Putra, A. Ikram, Bharoto, E. Santoso, T. C. Fang, N. Ibrahim and A. A. Mohamed, *AIP Conf. Proc.*, 2008, **989**, 130–133.
60 S. Jungblut, J.-O. Joswig and A. Eychmüller, *J. Phys. Chem. C*, 2019, **123**, 950–954.
61 C. E. White, D. P. Olds, M. Hartl, R. P. Hjelm and K. Page, *J. Appl. Crystallogr.*, 2017, **50**, 61–75.
62 I. Bressler, B. R. Pauw and A. F. Thunemann, *J. Appl. Crystallogr.*, 2015, **48**, 962–969.
63 Z. Wang, G. A. Craig, A. Legrand, F. Haase, S. Minami, K. Urayama and S. Furukawa, *Chem.–Asian J.*, 2021, **16**, 1092–1100.